Journal of Membrane Science 620 (2021) 118875

Contents lists available at ScienceDirect

Journal of Membrane Science

journal homepage: http://www.elsevier.com/locate/memsci

Upscaling polyPOSS-imide membranes for high temperature H_2 upgrading

Luca Ansaloni [a,*], Eric Louradour [b], Farzaneh Radmanesh [c], Henk van Veen [d], Monika Pilz [e], Christian Simon [e], Nieck E. Benes [c], Thijs A. Peters [a]

[a] Department of Sustainable Energy Technology, SINTEF Industry, Oslo, Norway
[b] CTI, ALSYS Group, Salindres, France
[c] Membrane Science and Technology Cluster, Faculty of Science and Technology, University of Twente, Enschede, the Netherlands
[d] Expertise Group Biomass & Energy Efficiency, Unit TNO-Energy Transition, Petten, the Netherlands
[e] Department of Materials and Nanotechnology, SINTEF Industry, Oslo, Norway

ARTICLE INFO

Keywords:
H_2 recovery
polyPOSS-imide
Membrane
Gas separation
Coke oven gas

ABSTRACT

In the present work, the potential of polyPOSS-imide membranes designed for the purification of H_2 from a coke gas (utilized in the steelmaking industry) is investigated. Aiming at upscaling the membrane fabrication, tubular single-channel and multi-channel membranes were prepared, using polyhedral oligomeric silsesquioxane (POSS) nanostructures and 6FDA as reactive precursors. The gas separation performance has been investigated by means of single gas and quaternary (H_2, CH_4, CO_2, N_2) mixtures, the latter used to simulate the conditions expected at the membrane module inlet in the process of upgrading H_2 from a coke oven gas. Preliminary results obtained on tubular membranes showed that the fabricated membranes can achieve high H_2 permeance (>2000 GPU), displaying also suitable selectivity towards CO_2, N_2 and CH_4. The selectivity of these upscaled tubular membrane samples meets the performance of those previously obtained for the disc-shaped lab-scale membranes. These results revealed the promising potential in the upscaling of polyPOSS-imide membranes fabricated via interfacial polymerization on ceramic porous supports for H_2 upgrading.

1. Introduction

The growing concerns on climate changes and the limited availability of fossil fuels worldwide is expected to lead to fundamental changes in the energy sectors. Climate neutrality [1] is now on the agenda of most of the global governments, and carbon-rich energy carriers are expected to be phased out and be replaced with more sustainable solutions. Hydrogen can store and deliver a considerable amount of energy and its carbon-free nature makes it the most attractive option as energy carrier and electricity storage to pursue the achievement of a more sustainable society in the future. H_2-related energy technologies have been studied in the last decades, but in recent years hydrogen underwent a very positive momentum which is expected to set it on path to deploy the hydrogen economy [2]. A recent report from the European Chemical Industry Council (Cefic) [3] identified hydrogen as a key player for the transition to low carbon electricity and low carbon industrial processes. Especially in the long-term, a complete elimination of fossil fuels in transport and industry without resorting to hydrogen may be hard to achieve. In the IEA 2DS–high H_2 scenario [4], a significant increase in the H_2 use is therefore projected, from the current annual energy use of ca. 7 EJ to nearly 30 EJ in 2050.

Hydrogen is today mainly produced from reforming reactions of steam with fossil feedstocks, with close-to 50% from natural gas. Other feedstocks include crude oil and coal [5]. Currently, the global CO_2 emissions associated with H_2 production are ~830 Mt CO_2/y [2]. Assuming business-*as*-usual a yearly CO_2 emission of over ~2 Gt is estimated for 2050 [4]. This can be reduced through a combination of hydrogen produced by electrolysis with renewable electricity, so-called Green H_2, and by reforming of fossil fuels with carbon capture and storage, so-called Blue H_2. However, in many industrial processes, hydrogen is produced as a by-product and its recovery can open up new business opportunities as well as facilitate the deployment of the H_2 society, which is still in its early stage [6]. Gas purification technologies need typically to be implemented to achieve the required H_2 purity depending on the process. In the case of chloralkali off-gas, hydrogen is obtained at relatively high purity (90–95% [7]), whereas in the case of ammonia purge gas, a higher H_2 dilution can be expected (H_2 content ~60% [8]). Surplus H_2 can also be found in blast furnace gas (BFG) and

* Corresponding author.
E-mail address: luca.ansaloni@sintef.no (L. Ansaloni).

https://doi.org/10.1016/j.memsci.2020.118875
Received 28 July 2020; Received in revised form 14 October 2020; Accepted 27 October 2020
Available online 3 November 2020
0376-7388/© 2020 The Authors. Published by Elsevier B.V. This is an open access article under the CC BY license (http://creativecommons.org/licenses/by/4.0/).

coke oven gas (COG) from the iron and steel making process. For the BFG direct H_2 recovery is not profitable due to the low H_2 content (~5 mol% [9]). On the contrary, COG process contains a large amount of H_2 (~60 mol% [9]) and has been proposed as an alternative hydrogen source, instead of using only its heating value [10].

Pressure swing adsorption and membrane separation have been the two main technologies proposed for hydrogen separation from COG, although other possibilities have also been investigated including hydrate formation and cryogenic separation [11]. Important benefits of membrane systems are related to their operational flexibility, combined with low energy consumption, small footprint, and cost-effectiveness. Polymeric membranes are the most commonly used membranes in the field of gas separation [12], but limitations of polymeric membranes include their susceptibility to swelling and plasticization and their modest thermal stability; only a few membrane materials are able to operate for long times at elevated temperatures [13,14]. Metallic membranes for hydrogen separation can be operated at high temperature, typically in the range 300–550 °C, becoming the preferred solution for H_2-rich streams coming from Water Gas Shift (WGS) reactors [15,16]. In the intermediate temperature range (typically 100–300 °C), microporous silica, zeolite membranes, or carbon membranes are envisioned, but perhaps the biggest challenge that is faced by all H_2 separation membranes is the lack of chemical stability. Water, sulphur-containing species, acidic vapours, and CO_2 are the most commonly encountered problematic contaminants which must be dealt with [17–20]. Further studies on developing novel and more stable membrane materials are thus required [21].

Polyimides (PIs) have been recently reported as suitable materials for H_2 purification [22]. PIs are typically characterized by high glass transition temperature (above 200 °C), making them attractive for high temperature gas separation applications such as the one involving H_2. Thanks to their glassy nature, they can achieve good separation of H_2 from N_2 and CH_4, but unfortunately the do not own high H_2/CO_2 sieving ability. Among the various approaches to overcome this problem, crosslinking has been demonstrated to be an effective technique to improve the separation performance of PIs. Recently, hyper-crosslinked nanoscale hybrid materials derived from alternating polyhedral oligomeric silsesquioxanes (POSS) and aromatic imide bridges (polyPOSS-imide) show promising performance for H_2 purification applications at elevated temperature [23,24]. Different dianhydrides can be used as organic ligands to form the selective layer structure, and 6FDA dianhydride (4,4′-(Hexafluoroisopropylidene)diphthalic anhydride) has exhibited promising performance obtained in comparison to other dianhydrides [23]. Ultrathin films (<100 nm [25]) obtained via interfacial polymerization on γ-alumina discs allowed to achieve high H_2 permeance while the inorganic nature of the POSS fraction enables persistence of the ability of molecular sieving at much higher temperatures as compared to traditional polymeric membranes. PolyPOSS-imide membranes retains gas selectivity of approximately 5 for H_2/CH_4 and H_2/N_2 at 300 °C, while still performing high H_2 permeance (>1000 GPU) [23]. Moreover, the CO_2/CH_4 selectivity of approximately 60 at temperatures below 100 °C emphasize the applicability of the polyPOSS−imide over a broad temperature range [24].

In the present work, the potential of novel polyPOSS-imide membranes for the recovery of H_2 from COG stream is investigated. Aiming at upscaling the membrane fabrication, tubular single-channel and multi-channel membranes were prepared, using commercial POSS nanoparticles and 6FDA as precursors. The membranes have been fabricated on the new porous supports following the synthesis procedure previously reported [24]. The performance of the fabricated membranes has been investigated in a wide range of operating conditions, looking both at the effect of operating temperature and pressure, and mixed gas permeation measurements are reported for polyPOSS-imide membranes for the first time.

2. Materials and methods

2.1. Membrane fabrication

Porous alumina disks were purchased from Cobra Technologies BV (Rijssen, The Netherlands). The disks are made of α-alumina (mean pore size = 80 nm, Ø = 25 mm, thickness = 2 mm), one side polished and coated with γ-alumina top layer (mean pore size = 3–5 nm).

CTI asymmetric TiO_2/Al_2O_3 single-channel and multi-channel tubular supports (single-channel OD = 10 mm, ID = 6 mm, length = 250 mm; multi-channel: OD = 25 mm, with 7 channels ID 6 = mm, length = 250 mm, with 10 mm enamel on both ends, see Fig. 1) are first coated with an internal zirconia microfiltration layer and top coated with a γ-alumina membrane (mean pore size = 3–5 nm).

Following the procedure reported by Raaijmakers et al. [24], polyPOSS-imide membranes were prepared by interfacial polymerization of water soluble ammonium chloride-functionalized POSS 0.9 wt% (octa-ammonium POSS, Hybrid Plastics) and a 0.075 wt% 4,4-(hexafluoroisopropylidene) diphthalic anhydride (6FDA, Sigma-Aldrich) solution in toluene. The partial conversion of ammonium to primary amino groups was achieved by addition of NaOH until the solution reached a pH of 9.9. Then γ-alumina tubular membranes were pre-wetted with the aqueous POSS solution for 15 min under a 500-mbar vacuum, followed by drying for 30 min at room temperature. Subsequently, a solution of the dianhydride in toluene was poured in the channels. After 5 min, the toluene was removed, and the samples were rinsed with acetone. The membranes were dried for 3 h in air atmosphere and heat treated for 2 h at 300 °C to achieve the conversion. The full reaction scheme is reported in the supporting information of the initial study on polyPOSS-imide membranes [24]. The resulting polyPOSS-imide network was simulated using molecular dynamics and its mechanical properties were characterized [26]. XPS data showing the elemental composition of the polyPOSS-imide selective layer have been previously reported [23,24]. In order to investigate the reproducibility of the fabrication procedure, multiple batches of membranes were fabricated out of which in total 6 membranes were tested in terms of gas transport properties. The membranes GEN1, GEN7, GEN8, GEN9, GEN11, GEN13 have been fabricated with the same process and have been selected for further characterization.

2.2. Membrane characterization

2.2.1. Material characterization

The membrane morphology was studied by scanning electron microscopy (SEM) using JEOL JSM-6010LA. Membrane samples for SEM analysis were obtained via fracturing the ceramic tubes. Secondary and back-scattered electrons were acquired at accelerating voltages of 5 kV, at low vacuum (80 Pa) conditions.

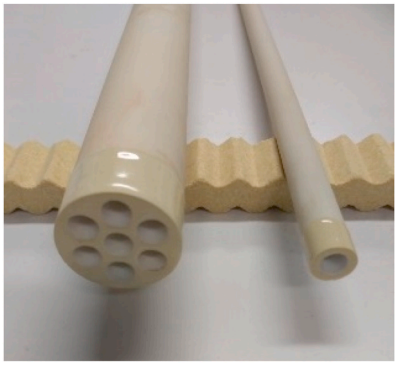

Fig. 1. Tubular ceramic multi-channel (left) and single-channel (right) prepared at CTI.

2.2.2. Gas permeation testing

The single-channel membranes were tested in a gas permeation rig available at SINTEF. The tubular samples were placed inside the module shown in Fig. 2, where Kalrez® 7075 O-rings (stable up to 327 °C) were used to seal the upstream from the downstream side of the membrane. Since the selective layer was coated on the inner wall of the tubular membrane, the feed gas was applied on the lumen (i.e. inner side of the membrane, Fig. 2). The effective permeation area was calculated assuming an effective length of 23 cm, as approximately 1 cm (on each side) was glazed and allowed for a proper sealing of the O-ring, resulting in an active permeation area of 43 cm^2. As shown in Fig. 2, the membrane performance was evaluated in a cross flow configuration (no sweep gas is used on the permeate side). Pure H_2 (99.995%), N_2 (99.999%), CO_2 (99.999%), CH_4 (99.95%) were delivered by AGA Norway.

The permeation system reported in Fig. 3 was used for the characterization of the single-channel tubular membranes. Mass flow controllers (MFC, Bronkhorst High-Tech B·V., The Netherlands) were used to accurately control the gas feed flow, allowing to achieve the required concentrations in the feed gas. The feed pressure is controlled by means of a back-pressure regulator (BPR, Bronkhorst High-Tech B·V., The Netherlands). The permeate stream is maintained at ambient pressure and the gas flowrate is measured by means of mass flowmeters (MFM, Bronkhorst High-Tech B·V., The Netherlands) measuring high (up to 40 L/min) and low (up to 2 L/min) flow. The membrane module is placed inside a furnace (ESTF 100/11, Entech, Sweden); besides the sensor for the temperature control of the furnace, an additional sensor was placed directly in the gaseous stream exiting the membrane module on the retentate side. All the MFCs and MFMs used in the characterization were initially calibrated using an automatic film flow meter (Horiba Stec VP-3, Horiba, Japan). The gas concentration in all the gaseous stream (feed, retentate and permeate) was measured by means of a micro GC (μGC, Agilent 490). All the parameters were logged with an in-house made LabView software.

The multi-channel membranes were tested in a gas permeation rig available at TNO, as shown in Fig. S1. The multi-channel membrane was fitted in a module (comparable to the one showed in Fig. 2) using Kalrez® 7075 O-rings and was placed in a temperature controlled oven (Carbolite HST12/600 with Eurotherm control). Feed was applied on the inside of the membranes that have a length of 25 cm and contains 7 channels with a diameter of 6 mm leading to an effective surface area of 289 cm^2. The membrane performance was evaluated in a configuration with a with small feed side bleed flow, as can be seen in Fig. S1. Pure H_2 (99.999%) and CO_2 (99.995%) were obtained from bottles supplied by Air Liquide. The process was controlled using MFC's (5 different controllers with an overlapping range between 0 and 50 L/min) and pressure indicators controllers (EL-FLOW and EL-PRESS, Bronkhorst High-Tech B·V., The Netherlands).

The gas permeance of the i-th gas, P_i, is calculated as reported by Equation (1):

$$P_i = \frac{\dot{n}_p \cdot y_{i,p}}{A \cdot \Delta p_i} \tag{1}$$

where $\dot{n}_p$ is the total molar gas flow on the permeate side calculated from the MFM measurement, $y_{i,p}$ is the i-th gas concentration in the permeate side, A is the membrane area and Δp_i is the differential partial pressure of species i between the feed/retentate and the permeate side (i.e., the driving force). In the case of single gas experiments, the Δp_i is calculated as:

$$\Delta p_i = p_{f,i} - p_{p,i} \tag{2}$$

where the indexes refer to the total pressure on the feed (f) and permeate (p) side respectively. In the case of gaseous mixture, due to the large permeance and the stage-cut reached in the experiment, the Δp is calculated as its logarithmic mean:

$$\Delta p_i = \frac{\left(p_{f,in} - p_p\right)_i - \left(p_{f,out} - p_p\right)_i}{\ln\left(p_{f,in} - p_p\right)_i - \ln\left(p_{f,out} - p_p\right)_i} \tag{3}$$

Where the $p_{f,in}$ and $p_{f,out}$ are the pressure at the feed inlet and outlet respectively.

The selective features of the membrane were evaluated by calculating the separation factor. In the case of gaseous mixtures, this value is calculated as the ratio between the gas concentration in the permeate (y) and in the feed (x) stream, as shown in Equation (4):

$$\alpha = \frac{y_i / y_j}{x_i / x_j} \tag{4}$$

where, i is the concentration of the fastest permeating component, while j is the concentration of the slower permeating component.

In the case of single gas experiments, the separation factor can be approximated to the permeance ratio as reported in Equation (5), referred as ideal selectivity value [27].

$$\alpha_{ideal} = \frac{P_i}{P_j} \approx \lim_{p_p \to 0} \alpha \tag{5}$$

As reported above, it is important to note that the ideal selectivity offers a good estimate of the real separation factor if the permeate partial pressure can be considered negligible compared to the feed one. In view of the extremely thin nature of the polyPOSS-imide-based selective layer coated on top of the porous support, this assumption may not be valid, possibly leading to a large deviation of the ideal selectivity from the separation factor.

For each separation experiment, the stage cut (which can also be referred to as H_2 recovery) was also calculated as the ratio between the

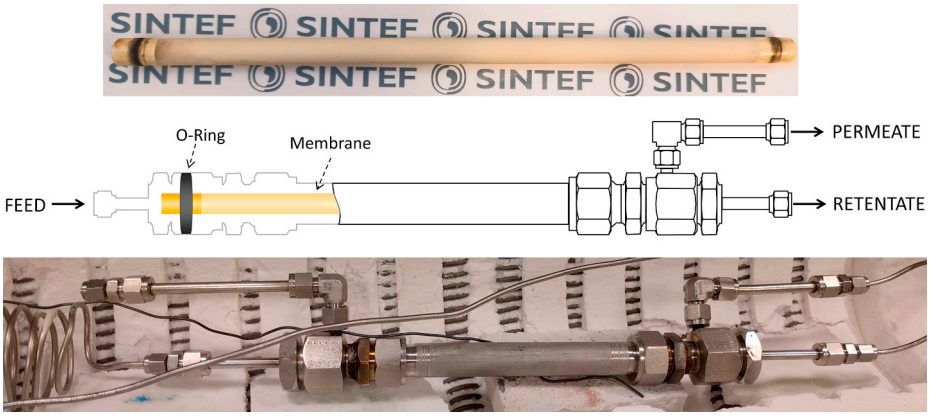

Fig. 2. PolyPOSS-imide tubular membrane and testing module.

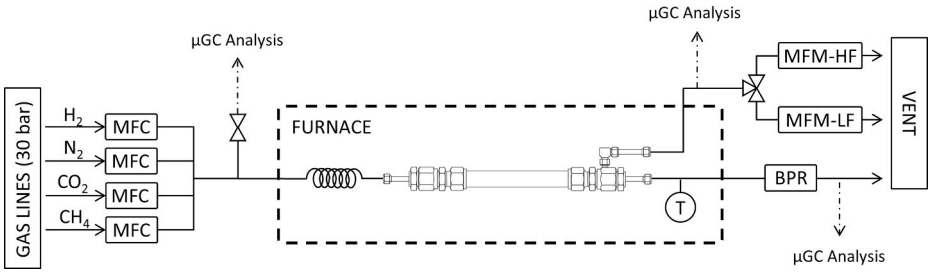

Fig. 3. Gas permeation test rig used at SINTEF (MFC = mass flow controller; MFM – HF = mass flowmeter high flow, MFM – LF = mass flowmeter low flow; BPR = back pressure regulator; T = temperature sensor).

gas flow on the permeate and on the feed side of the membrane:

$$stage\ cut = \frac{\dot{n}_p \cdot y_{i,p}}{\dot{n}_f \cdot y_{i,f}} \quad (6)$$

3. Results and discussion

3.1. Morphological characterization

Fig. 4 shows a cross-section of the inner side of the tubular membrane. The porous support constitutes of several microfiltration layers with different thicknesses and porosities (Fig. 4). A 7 μm thick γ-alumina layer is present on the top of the zirconia microfiltration membrane. The polyPOSS-imide layer is then coated atop, and the interfacial polymerization process allowed to keep the thickness of this selective layer between 100 and 200 nm (Fig. 4). This agrees well with the thickness obtained in a previous work applying α-alumina discs with a 3 μm-thick γ-alumina layer [24]. The membrane thickness is controlled by the contact time between the aqueous POSS and the dianhydride solution. As reported by Raaijmakers et al. [24], a contact time of 5 min is typically adequate to achieve a selective layer thickness of approximately 100 nm.

Fig. 5 shows the EDS mapping of the cross-section of the polyPOSS-imide membrane, also including a vertical line-scan extracted from the image. From the elemental analysis, it is possible to clearly see that the Si concentrated only in the top polyPOSS-imide layer, whereas the bottom layer (γ-alumina) is rich in Al. The poor resolution for both elements presented (Si and Al) is related to the resolution achievable by the instrument. The line-scan extracted from the image clearly show a peak of Si concentration around 0.6 μm from the top of the image, corresponding to the expected polyPOSS-imide layer position. The Al and O profile instead have an increase around 0.5 μm from the top and reach a constant intensity at 0.7 μm from the top of the image. Such profile remains then constant until the bottom, clearly identifying the bottom layer as γ-alumina.

3.2. Mass transport resistance of the porous support

According to the SEM analysis, extremely thin selective layers were obtained upon interfacial polymerization. At this thickness, the influence of the porous membrane on the mass transport resistance can become significant and requires a dedicated assessment. Therefore, the gas permeance of the porous tubular membranes was investigated. The tests were performed at various temperatures in the range of interest for the targeted application. Furthermore, pure H_2 and N_2 were used as feed gas, being the most and the least permeable (together with CH_4) gas, respectively, for the polyPOSS-imide membrane [23].

In the case of tubular membranes, in view of the large area and the consequent large permeate flow though the porous layer, the permeance was measured by monitoring the pressure drop created across the membrane for a given feed flow in a dead-end mode. The gas flow was varied between 1, 2 and 5 L/min, resulting in different differential pressures over the membrane. Equation (1) was used to calculate the permeance and the final value was averaged between these three measurements. As shown in Fig. 6 the H_2 permeance showed a decrease from 50,000 to 40,000 GPU within a temperature increase from between 100 and 300 °C. The observed temperature deactivation was expected in view of the Knudsen diffusion regime characterizing the transport in γ-alumina membranes as the Knudsen flux scales with $1/T^{½}$ (a factor of 1.25 is observed for the permeances, whereas $(T_{low}/T_{high})^{½}$ equals 1.24). In the case of N_2, a similar temperature effect was observed, but with a permeance drop from 16,000 to 12,000 GPU in the same temperature range. As shown in Fig. 6, the ideal H_2/N_2 selectivity is about 3.25, which is close to the expected Knudsen diffusion selectivity (approximately 3.7).

3.3. Single-channel polyPOSS-imide membrane performance

3.3.1. Pure gas permeation

Fig. 7 shows the pure gas permeance for H_2, N_2, CO_2, and CH_4 as function of temperature and transmembrane pressure obtained for membrane GEN7. As shown later in section 3.4.1, GEN7 is a membrane that shows a permeance at the lower side of the obtained variation

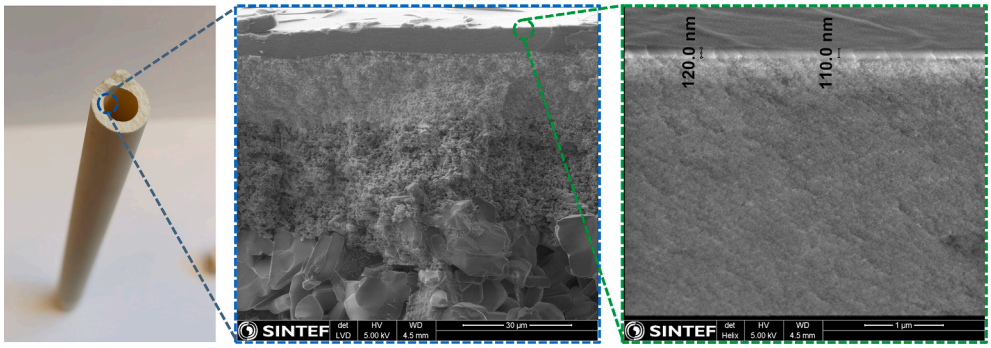

Fig. 4. SEM imaging of the cross-section of the single-channel polyPOSS-imide membrane.

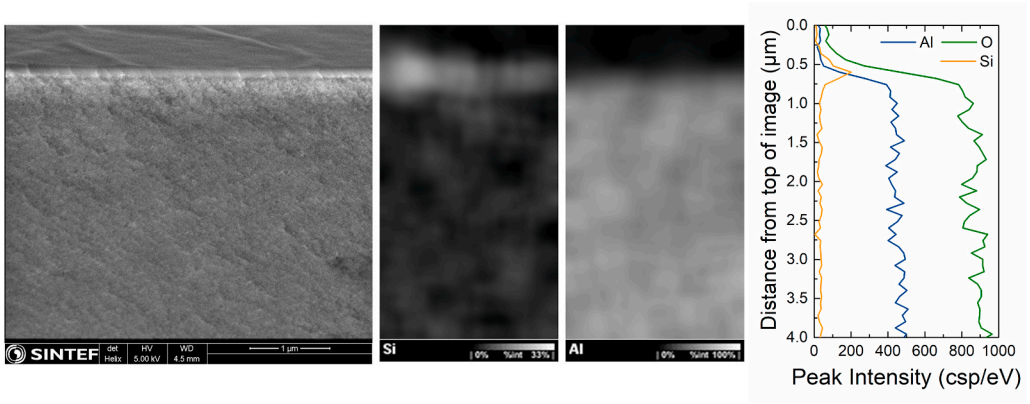

Fig. 5. EDS mapping of the cross-section of the single-channel polyPOSS-imide membrane.

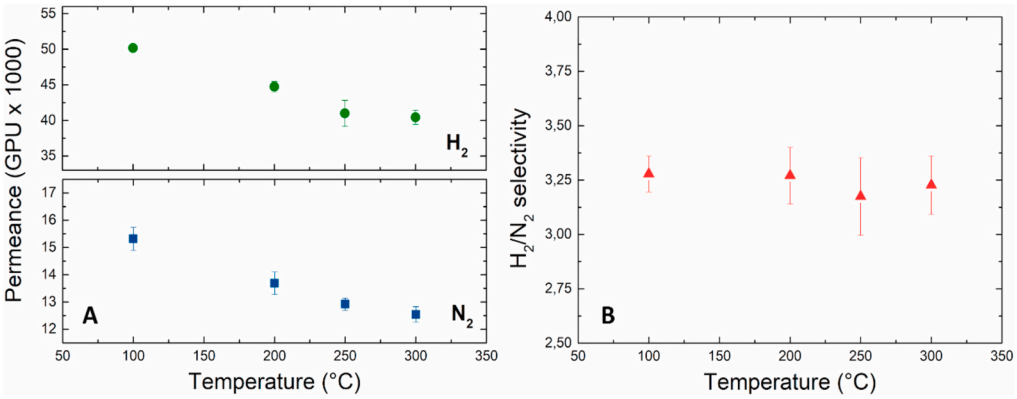

Fig. 6. Gas permeance (A) and ideal selectivity (B) obtained for the uncoated single-channel γ-alumina tubular membrane using pure gas as feed.

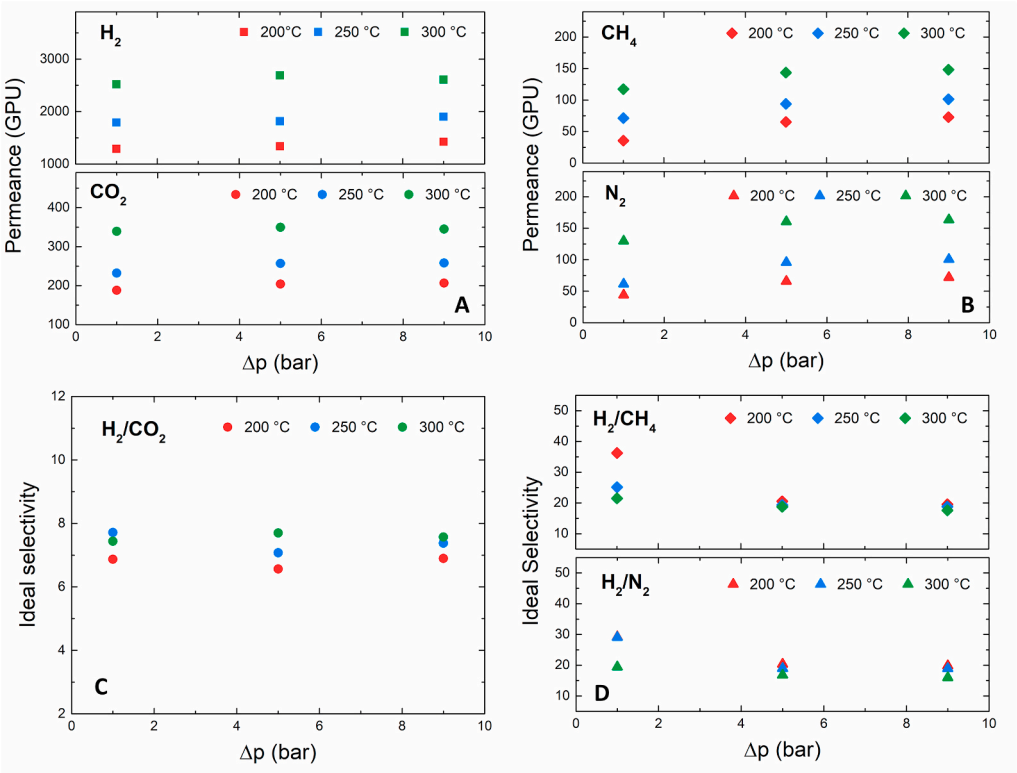

Fig. 7. Influence of pressure and temperature on the pure gas transport properties of polyPOSS-imide single-channel membrane.

among the membranes evaluated within this study. Consequently, the selectivity is on the high end of the observed variation. Still, we regard this sample as being representative for the produced membranes and a thorough characterization of the transport properties for this membrane sample is therefore presented below.

In the case of H_2, the permeance is found to increase from ~1400 GPU to ~2600 GPU in the investigated temperature range and appears to be relatively independent on the pressure for the considered range (2–10 bar). The CO_2 permeance ranges with temperature from ~200 to ~350 GPU, whereas N_2 and CH_4 vary from ~70 to ~150 GPU. It is interesting to notice that the permeance of all gases measured for the polyPOSS-imide selective layer is at least a factor of 15 lower than the support, clearly indicating that the contribution of the support to the mass transfer resistance is negligible. Therefore, the support is expected to have insubstantial effect on the gas transport behavior, despite the ultrathin nature of the selective layer. The permeance increases with temperature for all the gases, clearly showing a thermally activated gas transport, which is in line with results previously reported in literature [24]. For CH_4 and N_2, the ideal gas selectivity over H_2 is seemingly affected by the operating temperature only at low pressure, whereas negligible differences are measured at a feed pressure above 6 bar. Negligible influence is observed also for the H_2/CO_2 selectivity. At a temperature of 300 °C and 10 bar feed pressure, hydrogen and methane fluxes are 2610 and 148 GPU, respectively, resulting in a H_2/CH_4 selectivity of approximately 18. For the same temperature and pressure, the obtained H_2/CO_2 and H_2/N_2 selectivity are 7.6 and 16, respectively. The comparison of the H_2 permeance and H_2/N_2 selectivity (40,000 GPU and 3.25, respectively; Fig. 6) obtained for the porous support at 300 °C and the H_2 permeance and H_2/N_2 selectivity (2500 GPU and 15 to 20, respectively; Fig. 7) achieved for the polyPOSS membrane clearly indicates that the application of the polyPOSS-imide layer led to a strong increase of the separation performance. The coating of the selective layer also determined the change in the mechanism controlling the gas transport through the membrane, with solution-diffusion mechanism dominating over Knudsen diffusion.

Fig. 8 depicts the permeance on a logarithmic scale as a function of the inverse temperature (Arrhenius plot), confirming that the gas permeance is thermally activated. The activation energies (E_a) for the measured gases are in the order $N_2 > CH_4 > H_2 > CO_2$. The differences observed in terms of activation energies are related to the kinetic and thermodynamic feature of the gases as well as by their interaction with the polyPOSS-imide matrix. In general, the permeation of gases with larger kinetic diameters (N_2 and CH_4) is more temperature-sensitive, leading to a higher activation energy of permeation. However, for soluble gases (CO_2 and CH_4), the negative contribution of the enthalpy of sorption [28] is larger, partially reducing the activation energy value. Nevertheless, the values are quite similar for the investigated gases, which is in line with the negligible effect of temperature on the membrane selective feature (Fig. 7) and with a previous study of polyPOSS-imide fabricated with different dianhydrides [23]. In the case of H_2, the activation energy is similar (13.6 vs 11.2 kJ mol^{-1}) to the one previously reported by Raaijmakers et al. [24] for lab-scale disc-shaped membranes. The moderately higher value obtained in the present work could be related to the reduced mass transport resistance of the tubular membrane compared to the disk (Fig. S2) and to the higher operating pressure. As showed by Raaijmakers et al. [24], N_2 and CH_4 showed similar values which are the highest for the considered gases. However, the values are considerably lower than previously reported (15.9 vs 33.3 kJ mol^{-1} for CH_4, 18.4 vs 31.7 kJ mol^{-1} for N_2), showing that the transport mechanism for these gases is affected by temperature to a lower extent. On the contrary, CO_2 showed an increase in the Ea value (11.5 vs 3.7 kJ mol^{-1}). Such differences are likely related to the polyPOSS-imide structure, suggesting that minor structural changes can affect the temperature effect on the gas transport properties of the selective layer.

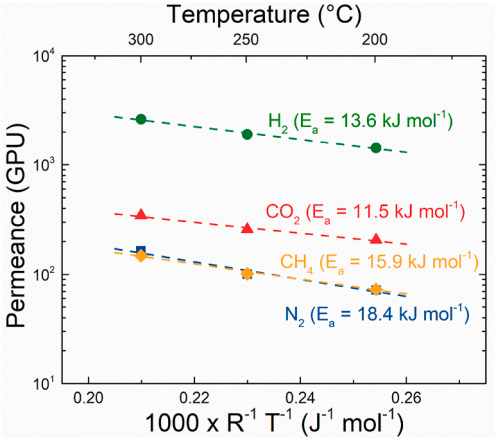

Fig. 8. Arrhenius plot of individual gas permeances for H_2, CO_2, N_2 and CH_4 (feed pressure = 10 bar). The activation energies are reported (regression coefficient is always larger than 98.8%).

Fig. 9 shows a comparison between the performance of the tubular polyPOSS-imide membrane with literature results presenting the initial work on the development of polyPOSS-imide membranes with similar organic ligand, but on small porous disc supports [23]. The FTIR characterization (Fig. S3), clearly showed very similar results to the one previously reported by Raaijmakers et al. [24]: the band corresponding to the *N*–H bending at 1620 cm^{-1} is not present anymore, while a sharp peak appeared at 1720 cm^{-1} (C═O stretching), confirming the successful fabrication of the polyPOSS-imide structure. Also the thermal properties (Fig. S4) appeared to be similar to the one previously published [24], showing stability up to 300 °C. It can be observed that the performance of the tubular membrane (area = 43 cm^2) agrees well with the performance of the disc-shaped membranes (area = 1.5 cm^2). In fact, even a higher hydrogen permeance is obtained, which is explained by the lower resistance for mass transport in the tubular supports compared to the disk-shape supports. The tubular supports present a different morphological structure with respect to the disk (Fig. S5), resulting in one order of magnitude lower resistance to the gas transport (Fig. S2), which can easily explain the higher permeance obtained for the current tubular polyPOSS-imide membranes [29]. For H_2 at 200 °C, the resistance of the tubular support is about 12 folds the one obtained for the disk (17 vs 213 s/m for tubular membrane and disk respectively). At 300 °C, the difference in permeance with respect to literature is even more evident, due to the larger H_2 flux obtained at higher temperature. As expected, this effect becomes less evident for less permeable gases, due to the lower transmembrane flux obtained. Consequently, the higher hydrogen permeance determines higher values for the ideal selectivity ($\Delta p = 1$ bar). An increase with a factor between 1.7 and 2 is observed in the case of the H_2/CO_2 ideal selectivity; even larger increments were observed for H_2/N_2 (1.8–4.5 folds) and H_2/CH_4 (1.5–3.4 folds). Overall, this comparison shows that the facile synthesis of interfacial polymerization followed by thermal imidization is as well applicable to tubular supports and thus shows potentially for large-scale production of this type of membrane.

3.3.2. *Mixed gas permeation*

Fig. 10 shows the performance of membrane GEN7 using quaternary gas mixtures at various temperatures (200, 250 and 300 °C) and total pressures (4 and 10 bar). For all the operating conditions considered, a gaseous mixture containing 60% H_2, 20% CH_4, 10% N_2 and 10% CO_2 was used to mimic the conditions of the coke oven gas. In addition, other two gaseous mixture with decreasing H_2 content (40% H_2, 30% CH_4, 15% N_2 and 15% CO_2 and 20% H_2, 40% CH_4, 20% N_2 and 20% CO_2) were considered, to account for the H_2 recovery occurring in real-size separation modules. The tests were normally left to stabilise for about 4 h. Longer-term testing showed that the results obtained after this

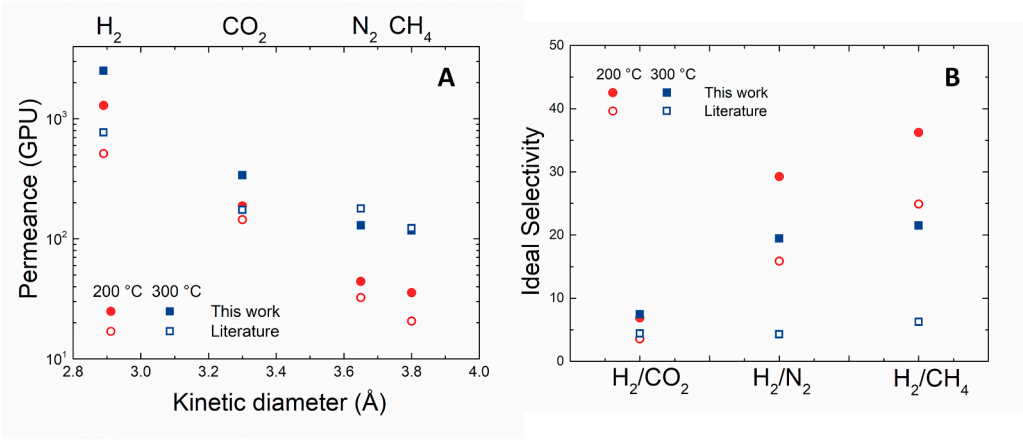

Fig. 9. Comparison of tubular polyPOSS-imide membrane in terms of gas permeance (A) and selectivity (B) with literature results [24] obtained on porous disk (feed pressure = 2 bar).

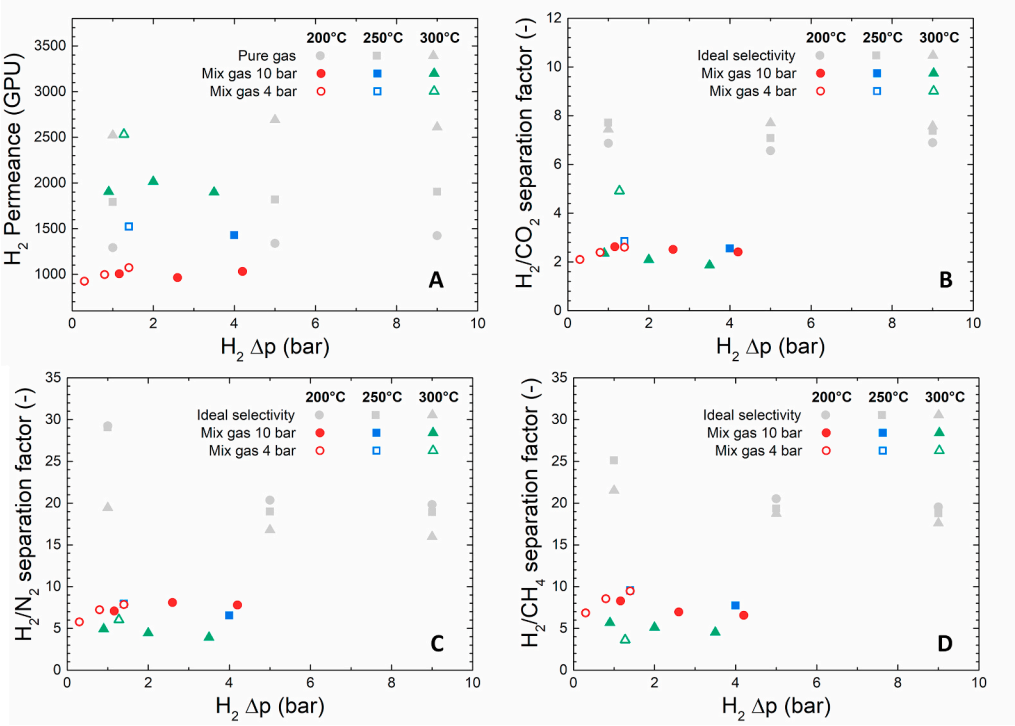

Fig. 10. PolyPOSS-imide separation performance using quaternary gas mixtures at various temperatures, pressures and gas concentration. For a given mix gas condition in terms of pressure and temperature, the presence of more than one points refer to different gaseous mixtures used as feed, with decreasing H_2 content).

period of time are representative over at least 60 h operation (Fig. S6).

Within the investigated temperature range, the H_2 permeance is partially affected by the presence of other gases in the feed mixture: at 10 bar, a drop of about 15–20% compared to the pure gas conditions is observed at 200 and 250 °C, increasing to 25–30% at 300 °C. This may be explained in terms of concentration polarization at the gas/membrane interface on the feed side. In view of the extremely high H_2 permeance and relatively high H_2 selectivity of the selective layer, a fast H_2 depletion occurs at the boundary layer, resulting in an increase of the local concentration of the other gases. A similar effect has been observed also in the case of Pd–Ag membranes for H_2 separation [30,31]. As observed for the pure gas experiments, the overall pressure has a limited effect on the H_2 permeance with minor differences observed between 10 and 4 bar, except for the test performed at 300 °C. In this case, the H_2 permeance measured at 4 bar is similar to the one obtained in the single gas test, whereas at 10 bar a 25% drop is observed. Interestingly, also the variation of the H_2 content in the gaseous feed had limited effect on the H_2 permeance, independently from the operating temperature. The permeance of CO_2 and CH_4 are observed to be in line with the pure gas experiments when plotted against the actual driving force (Δp) across the membrane, with a minor positive deviation (typically within 10%) observed at the different operating conditions. Contrarily, a relevant increase in N_2 permeance is systematically observed for all the experiments performed, with an average 2-fold increment within the considered operating range (Table S1). This effect may be associated with the simultaneous presence of CO_2 and CH_4 that have been previously reported to be able to induce significant swelling on the polyPOSS-imide matrix [32]. Being N_2 the least soluble gas of the mixture, swelling phenomena can affect its permeance to a larger extent resulting in higher N_2 permeance when evaluated in gaseous mixtures.

As a consequence of the above, the separation factor for all the gas pairs of interest is significantly lower than the ideal selectivity. In the case of H_2/CO_2, the value decreased from 7 obtained with pure gases to 2.5 obtained using mixtures (~65% drop). H_2/N_2 and H_2/CH_4 showed similar trends, with selectivity dropping from 20 obtained under pure gas to values between 8 and 10 (~55% drop). The effect appeared independent from the operating temperature, although at 300 °C it seemed to be slightly more pronounced, especially for the selectivity towards the less permeable gases (N_2 and CH_4). To exclude any effect of the stage cut on the measured performance, permeation tests at various feed flow rates were performed (Fig. 5S). The separation performance reported in Fig. 10 have been obtained using a total feed gas flow of 3000 ml/min, resulting in a 53% stage cut (feed pressure = 10 bar). The total feed flow rate was therefore increased to 5000 and 7000 ml/min reducing the stage cut to 33 and 23% respectively. However, only a minor increase (up to 20% of the initial value) could be observed in terms of H_2/N_2 and H_2/CO_2 selectivity (Fig. S7). A similar test was repeated also using a feed pressure of 4 bar. The lower driving force at this pressure condition determined a lower initial stage cut, corresponding to a value of 18%. By increasing the total feed flow rate to 4000 and 5000 ml/min, the stage cut was further reduced to 14% and 11% respectively. However, the selective feature of the membrane appeared to be negligibly affected by such change, clearly suggesting that the stage cut of the experiment was not responsible for the drop in separation factor.

To better understand the performance obtained using mixed gases, a 1-D model able to account for the depletion of the gas on the feed side was developed, assuming steady state conditions and homogeneous phase on the permeate side. The model is based on a finite element method (Fig. S8) and the transmembrane flux $J_i(x)$ is measured using the gas permeances obtained in the single gas experiments. The feed flow concentration of each gas (F_i) is allowed to change along the module length, maintaining the overall feed pressure constant. Due to the high H_2 permeance and relatively large membrane area, the H_2 content in the feed side decreased to a large extent, whereas the other gases increased along the active membrane area. Fig. S9 shows the case at 200 °C. The H_2 concentration dropped from 60 mol% at the inlet to 35 mol% at the outlet (Fig. S9A), impacting the H_2 driving force and consequently the H_2 flux across the selective layer (Fig. S9B). On the other hand, the content of CO_2, CH_4 and N_2 increases by 45%, 65% and 65%, respectively. The higher driving force generated along the module led to an increase of the transmembrane flux for these gaseous species, resulting in a dilution of the gas phase in the permeate side. The predicted gas compositions of the permeate stream obtained at the outlet of the membrane module are compared with the experimental data in the parity plot shown in Fig. 11. Despite minor deviations, possibly related to the GC measurements or to concentration polarization phenomena, the data predicted using the gas permeances from single gas experiments correlate nicely with the ones obtained from mixed gas tests, independently from the operating temperature. Therefore, the gap between the ideal selectivity and the separation factor reported in Fig. 10 is simply related to the difference between a material performance (ideal selectivity) and a module performance (separation factor). The first one is simply dependent on the material characteristics, whereas the latter accounts also for the stage cut and the module configuration.

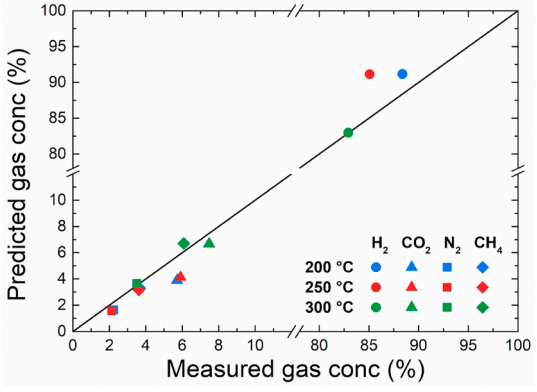

Fig. 11. Parity plot comparing the permeate compositions obtained experimentally with the model prediction (feed pressure: 10 bar; feed gas composition: 60% H_2, 20% CH_4, 10% N_2 and 10% CO_2).

3.4. Industrial upscaling

3.4.1. Reproducibility of single-channel polyPOSS-imide membranes performance

Fig. 12 contains permeance data for two batches of polyPOSS-imide membranes. These batches were made over a period of 8 months, and each batch consists of 7 membranes from which at least 2 membranes were tested. For all the investigated membranes, the H_2 permeance is negligibly affected by the operating pressure in the investigated range, while showing a temperature activated behavior. In the current study, total 6 membranes were tested more thoroughly with various gaseous species, 5 of them show a similar behavior. Only GEN11 showed an extraordinarily high permeance (as high as 5300 GPU), while maintaining decent selective features. The variation in permeance between the various membranes are likely due to differences in the polyPOSS-imide selective layer thickness. Measurements of the weight gain before and after the deposition of the selective layer partially point in this direction: for example, GEN7 and GEN 11 show the lowest and highest permeance as well as the highest and lowest weight gain, respectively (Table S2). However, for samples like GEN1 and GEN13, a larger permeance is observed despite the higher weight gain, possibly suggesting that the formation of minor surface defects may also play a role. From Fig. 12, it can be concluded that the typical hydrogen permeance of the polyPOSS-imide membranes is between 1500 and 2000 GPU at 200 °C. Fig. 13 shows the ideal selectivity obtained for pure and mixed gas experiments from the various samples. The ideal selectivity of H_2/CO_2, H_2/N_2, H_2/CH_4 is approximately 5–7, 10–20 and 9–20, respectively at 200 °C. Following the typical membrane trade-off, the samples showing larger H_2 permeance showed also lower selectivity. The variation in pure gas selectivity in the case of H_2/N_2 (6–20) and H_2/CH_4 (5–20) is larger than in the case of H_2/CO_2 (5–7). Minor defects on the surface may be responsible for the different N_2 and CH_4 selective feature of the membranes. Their effect is reduced for the gas with a smaller kinetic diameter (i.e. CO_2) and at higher operating temperatures, as their permeance is higher and thus the influence of Knudsen flow through defects is smaller. This is consistent with the fact that the share of the transmembrane flux associated to the leak is reduced at higher temperature (assuming a viscous flow behavior), while the contribution of defect-free area increases in view of the larger permeance.

In the case of H_2/CO_2, the selectivity is also reported to increase with temperature. This is in line with literature results [24] and clearly show that, for the given gas pair, the gas solubility plays a major role. However, it is interesting to notice that compared to the performance obtained on disks [24], most of the membranes show an increasing trend for the H_2/N_2 and H_2/CH_4 selectivity with temperature. The only exception is GEN7, where the H_2/N_2 and H_2/CH_4 selectivity drops from 20 to about 16 and 18 for N_2 and CH_4, respectively. As previously mentioned, GEN7 is expected to be the thickest membrane in the batch, possibly ensuring a defect-free nature of the selective layer. This may also confirm that thin selective layers of the other membranes in the batch present minor defects on the membrane surface, leading to different results in terms of selectivity. However, operations at temperatures above >200 °C may be enough to ensure a limited effect of the minor defects in the selective layers on the overall membrane performance.

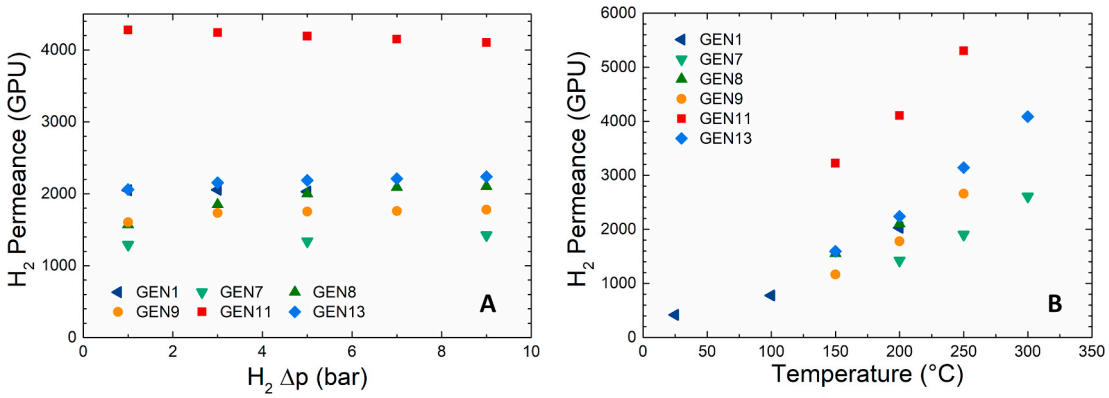

Fig. 12. H_2 permeance as function of pressure (A, T = 200 °C) and temperature (B, feed p = 10 bar) for various polyPOSS-imide membranes prepared in the study.

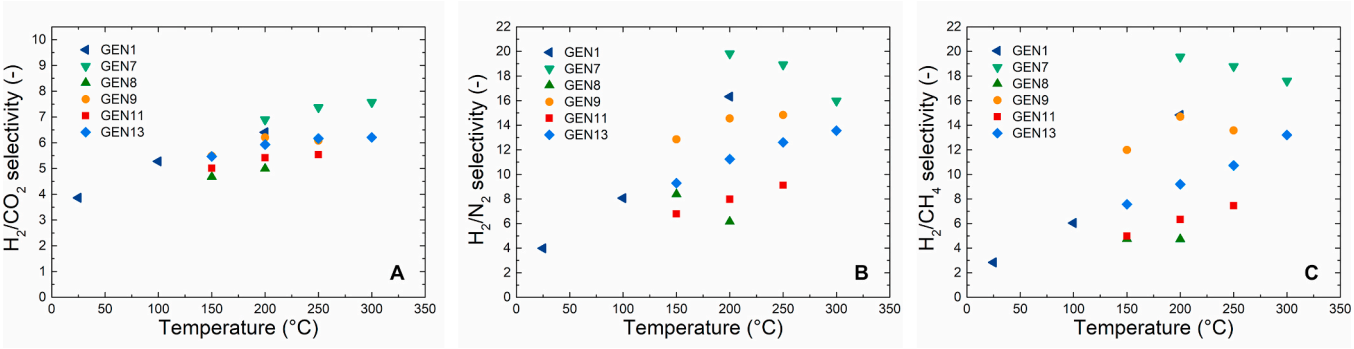

Fig. 13. H_2/CO_2 (A), H_2/N_2 (B) and H_2/CH_4 (C) selectivity as function temperature for various polyPOSS-imide membranes prepared in the study (feed p = 10 bar).

3.4.2. Aging

An important aspect of membrane upscaling is related to the investigation of aging phenomena that can potentially lower the membrane performance over time. In Fig. S6, stable operations were reported for the polyPOSS-imide membrane over a period of 60 h (operating temperature = 200 °C; operating pressure = 10 bar), showing promising results. In addition, the membrane performance was investigated after 14 months from the initial testing. During this period of time, the membrane was stored in the lab at ambient conditions. Fig. 14 displays the results obtained for pure gas testing, clearly showing a limited aging for the polyPOSS-imide. Within the pressure range investigated, the aged sample performed similarly to the pristine one, with negative drops limited to a maximum of 10% of the initial measurement.

3.4.3. Multi-channel polyPOSS-imide membrane performance

In the upscaling, a further effort was devoted to the demonstration of multi-channel membrane (7 channels, area = 289 cm^2) elements onto which a similar thin polyPOSS-imide selective layer was coated. Fig. 15 shows the performance obtained for the multi-channel membrane module obtained at TNO facilities and the comparison with the performance observed for the single channel membrane at SINTEF (Table 1 reports the performance obtained at all the tested conditions). The gas transport in the multi-channel membrane showed the same temperature activated behavior observed in the single-channel testing, and very similar temperature trends are identified for both for H_2 and CO_2. As expected, the SEM analysis performed on the sample (Fig. S10) shows a similar morphology compared to the single-channel. In the case of the multi-channel membrane, the activation energy of permeation is

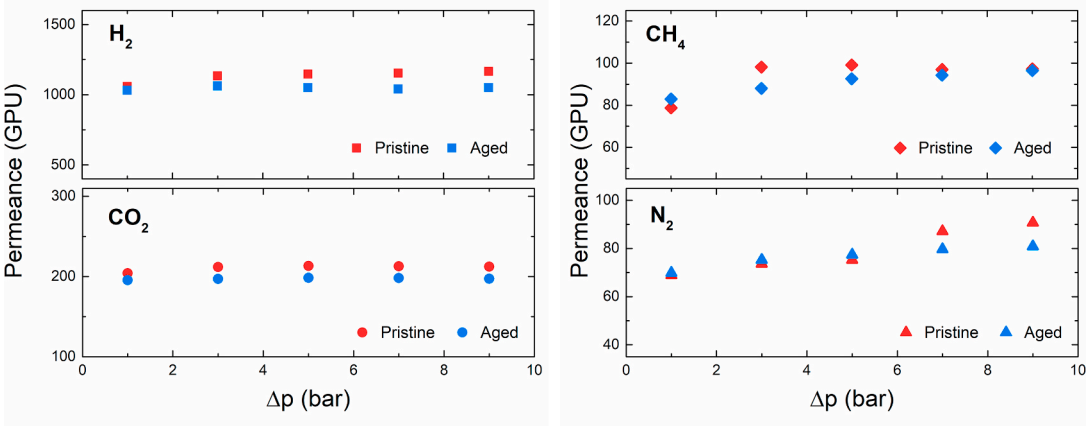

Fig. 14. Pure gas permeance of GEN9 after 14 months aging (operating temperature = 150 °C).

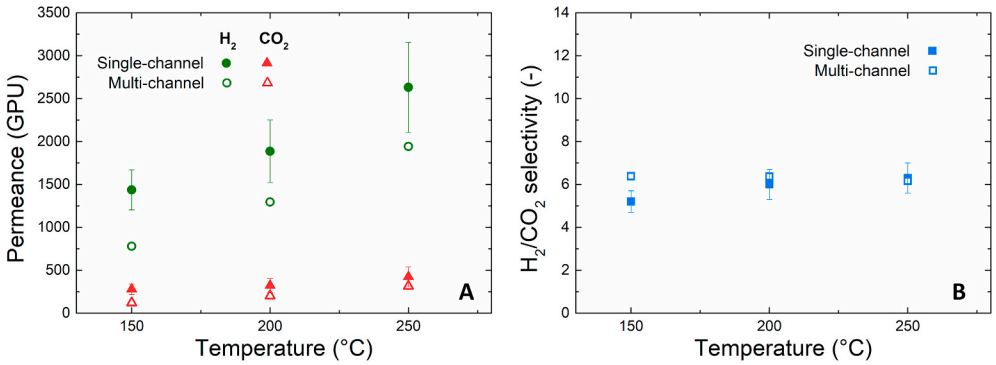

Fig. 15. Comparison between the performance of single-channel and multi-channel membrane at various temperature (feed pressure = 10 bar; the data for the single channel performance are the average of the representative samples from Figs. 12 and 13).

Table 1
Comparison of the gas separation performance between multi-channel and single-channel membranes at various temperature and pressure (the data for the single-channel performance are the average of the representative samples from Figs. 12 and 13).

	Multi-channel			Single-channel		
	Permeance		Sel	Permeance		Sel
P	H_2	CO_2	H_2/CO_2	H_2	CO_2	H_2/CO_2
bar	GPU	GPU	-	GPU (±)	GPU (±)	-
150 °C						
2	717	120	6.0	1202 (135)	242 (33)	5.0
6	762	120	6.4	1368 (217)	277 (59)	5.0
10	779	122	6.4	1437 (235)	279 (61)	5.2
200 °C						
2	1182	189	6.2	1715 (333)	284 (71)	6.1
6	1232	197	6.2	1862 (331)	312 (73)	6.1
10	1294	203	6.4	1886 (364)	322 (83)	6.0
250 °C						
2	1807	297	6.1	2547 (525)	387 (114)	6.7
6	2034	311	6.5	2597 (557)	418 (110)	6.3
10	1943	315	6.2	2547 (520)	424 (105)	6.3

calculated to be 16.8 and 17.4 kJ mol^{-1} for H_2 and CO_2 respectively, which are quite similar to the one reported in Fig. 8 for the GEN7 membrane. The H_2 permeance for the multi-channel module is observed to be about 35% lower than the average value obtained in the single-channel case, but the performance aligns properly with the one obtained for GEN7. At 250 °C and 10 bar, a H_2 permeance of approximately 2000 GPU has been achieved for the multi-channel, while still showing the same selective features. Interestingly, the H_2/CO_2 selectivity measured from pure gas experiments for both single- and multi-channel overlap nicely in the investigated temperature and pressure range, suggesting that the permeance differences may be simply related to the thickness of the selective layer achieved in the fabrication. It should be noted that the multi-channel support may also determine a higher resistance to the transport, leading to a lower permeance. Unfortunately, due to the extremely high transmembrane fluxes, it was not possible to determine this value as in the case of the single-channel. Furthermore, due to the geometrical configuration of the support, the central channel and the channel's walls facing it could be affected by a larger transport resistance compared to the single-channel case, possibly reducing the effective permeation area.

4. Conclusions

The potential of novel polyPOSS-imide membranes for the recovery of H_2 from COG gas stream has been investigated. Aiming at upscaling the membrane fabrication, tubular single-channel and multi-channel element membranes were prepared, using POSS and 6FDA molecules as precursors. The performance of the fabricated membranes has been investigated in a wide range of operating conditions, looking both at the effect of operating temperature and pressure. Mixed gas permeation measurements are reported for polyPOSS-imide membranes for the first time.

For the most selective membrane (GEN7), at 300 °C and 10 bar, hydrogen and methane permeance are 2610 and 148 GPU, respectively, resulting in a H_2/CH_4 selectivity of approximately 18. For the same temperature and pressure, the obtained H_2/CO_2 and H_2/N_2 selectivity are 7.6 and 16, respectively. The H_2 permeance is partially affected by the presence of other gases in the feed mixture: a drop of about 15–20% compared to the pure gas conditions is observed at 200 and 250 °C, increasing to 25–30% at 300 °C. This may be explained in terms of concentration polarization at the gas/membrane interface on the feed side. The separation factor for all the gas pairs of interest, however, decreased significantly. In the case of H_2/CO_2, the value decreased from about 7 obtained with pure gases to about 2.5 obtained using mixtures. The gap between the ideal selectivity and the separation factor are related to the difference between a material performance (ideal selectivity) and a module performance (separation factor). The first one depends on the material characteristics, whereas the latter accounts also for the stage cut and the module configuration.

The performance of the upscaled tubular polyPOSS-imide membranes agrees well with the performance of the lab-scale disk-shaped membranes. In fact, even a higher hydrogen permeance is obtained, which is explained by the lower resistance for mass transport in the tubular supports as compared to the disk-shape supports. The reproducibility of production was shown through the manufacturing of several batches of tubular polyPOSS-imide membranes. In total 6 membranes were tested out of which 5 show a similar behavior. Differences in permeance between the different membranes are likely due to differences in the polyPOSS-imide selective layer thickness and possibly due to minor defects in the selective layer. The latter effect appeared to be reduced by increasing the operating temperature, revealing that at temperature above 200 °C the presence of such defects has a minor influence on the membrane performance.

Finally, multi-channel membrane elements were also fabricated and tested. Despite the increase of 2 orders of magnitude in terms of permeation area (from 1.5 to 289 cm^2), the separation performance has been observed to exceed the one initially measured for lab-scale disk samples, clearly showing that the fabrication approach adopted owns a great up-scalability potential.

Funding

This work is part of the GENESIS project and the authors acknowledge the financial support from the European Union's Horizon 2020 Research and Innovation Program under the Grant Agreement No. 760899. This publication reflects only the author's views and the

European Union is not liable for any use that may be made of the information contained therein.

Author statement

Luca Ansaloni: Conceptualization, Methodology, Investigation, Writing - Original Draft.

Eric Louradour: Resources, Investigation, Writing - Review & Editing.

Farzaneh Radmanesh: Investigation, Writing - Review & Editing.

Henk van Veen: Investigation, Writing - Review & Editing.

Monika Pilz: Funding acquisition, Resources, Investigation, Writing - Review & Editing.

Christian Simon: Funding acquisition, Writing - Review & Editing.

Nieck E. Benes: Funding acquisition, Supervision, Writing - Review & Editing.

Thijs A. Peters: Funding acquisition, Conceptualization, Methodology, Writing - Review & Editing.

Declaration of competing interest

The authors declare that they have no known competing financial interests or personal relationships that could have appeared to influence the work reported in this paper.

Acknowledgements

SINTEF would like to thank Dr Martin Fleissner Sunding for carrying out the SEM analysis. TNO would like to thank Raghavendra Sumbharaju for carrying out the gas permeation testing.

Appendix A. Supplementary data

Supplementary data related to this article can be found at https://doi.org/10.1016/j.memsci.2020.118875.

References

[1] European Parlament, What Is Carbon Neutrality and How Can it Be Achieved by 2050?, 2019 accessed, https://www.europarl.europa.eu/news/en/headlines/society/20190926STO62270/what-is-carbon-neutrality-and-how-can-it-be-achieved-by-2050. (Accessed 13 March 2020).

[2] IEA, The Future of Hydrogen (June 2019), 2019. https://www.iea.org/reports/the-future-of-hydrogen.

[3] The European Chemical Industry Council - Cefic, A Journey into the Future of Europe with the European Chemical Industry (June 2019), 2019. https://cefic.org/app/uploads/2019/06/Cefic_Mid-Century-Vision-Molecule-Managers-Brochure.pdf.

[4] IEA, Energy Technology Perspectives 2017, 2017. Paris, https://www.iea.org/reports/energy-technology-perspectives-2017.

[5] P. Nikolaidis, A. Poullikkas, A comparative overview of hydrogen production processes, Renew. Sustain. Energy Rev. 67 (2017) 597–611, https://doi.org/10.1016/J.RSER.2016.09.044.

[6] M. Yáñez, A. Ortiz, B. Brunaud, I.E. Grossmann, I. Ortiz, Contribution of upcycling surplus hydrogen to design a sustainable supply chain: the case study of Northern Spain, Appl. Energy 231 (2018) 777–787, https://doi.org/10.1016/J.APENERGY.2018.09.047.

[7] J. Benson, A. Celin, Recovering Hydrogen — and Profits — from Hydrogen-Rich Offgas, CEP Manazine, 2018. https://www.aiche.org/resources/publications/cep/2018/january/recovering-hydrogen-and-profits-hydrogen-rich-offgas.

[8] F. Siavashi, M. Saidi, M.R. Rahimpour, Purge gas recovery of ammonia synthesis plant by integrated configuration of catalytic hydrogen-permselective membrane reactor and solid oxide fuel cell as a novel technology, J. Power Sources 267 (2014) 104–116, https://doi.org/10.1016/J.JPOWSOUR.2014.05.072.

[9] W.-H. Chen, M.-R. Lin, T.-S. Leu, S.-W. Du, An evaluation of hydrogen production from the perspective of using blast furnace gas and coke oven gas as feedstocks, Int. J. Hydrogen Energy 36 (2011) 11727–11737, https://doi.org/10.1016/J.IJHYDENE.2011.06.049.

[10] W. Uribe-Soto, J.-F. Portha, J.-M. Commenge, L. Falk, A review of thermochemical processes and technologies to use steelworks off-gases, Renew. Sustain. Energy Rev. 74 (2017) 809–823, https://doi.org/10.1016/J.RSER.2017.03.008.

[11] J.M. Bermúdez, A. Arenillas, R. Luque, J.A. Menéndez, An overview of novel technologies to valorise coke oven gas surplus, Fuel Process. Technol. 110 (2013) 150–159, https://doi.org/10.1016/J.FUPROC.2012.12.007.

[12] E. Lasseuguette, M.-C. Ferrari, Polymer membranes for sustainable gas separation, Sustain. Nanoscale Eng. (2020) 265–296, https://doi.org/10.1016/B978-0-12-814681-1.00010-2.

[13] S.C. Kumbharkar, Y. Liu, K. Li, High performance polybenzimidazole based asymmetric hollow fibre membranes for H2/CO2 separation, J. Membr. Sci. 375 (2011) 231–240, https://doi.org/10.1016/J.MEMSCI.2011.03.049.

[14] X. Li, R.P. Singh, K.W. Dudeck, K.A. Berchtold, B.C. Benicewicz, Influence of polybenzimidazole main chain structure on H2/CO2 separation at elevated temperatures, J. Membr. Sci. 461 (2014) 59–68, https://doi.org/10.1016/J.MEMSCI.2014.03.008.

[15] K. Atsonios, K.D. Panopoulos, A. Doukelis, A.K. Koumanakos, E. Kakaras, T. A. Peters, Y.C. van Delft, Introduction to palladium membrane technology, Palladium Membr. Technol. Hydrog. Prod. Carbon Capture Other Appl. (2015) 1–21, https://doi.org/10.1533/9781782422419.1.

[16] T.A. Peters, P.M. Rørvik, T.O. Sunde, M. Stange, F. Roness, T.R. Reinertsen, J. H. Ræder, Y. Larring, R. Bredesen, Palladium (Pd) membranes as key enabling technology for pre-combustion CO2 capture and hydrogen production, Energy Procedia 114 (2017) 37–45, https://doi.org/10.1016/J.EGYPRO.2017.03.1144.

[17] T.A. Peters, T. Kaleta, M. Stange, R. Bredesen, Hydrogen transport through a selection of thin Pd-alloy membranes: membrane stability, H2S inhibition, and flux recovery in hydrogen and simulated WGS mixtures, Catal. Today 193 (2012) 8–19, https://doi.org/10.1016/J.CATTOD.2011.12.028.

[18] T.A. Peters, R. Bredesen, H.J. Venvik, CHAPTER 6 Pd-based membranes in hydrogen production: long-term stability and contaminant effects, in: Membr. Eng. Treat. Gases Vol. 2 Gas-Separation Issues Comb. With Membr. React., The Royal Society of Chemistry, 2018, pp. 177–211, https://doi.org/10.1039/9781788010443-00177.

[19] M. ten Hove, M.W.J. Luiten-Olieman, C. Huiskes, A. Nijmeijer, L. Winnubst, Hydrothermal stability of silica, hybrid silica and Zr-doped hybrid silica membranes, Separ. Purif. Technol. 189 (2017) 48–53, https://doi.org/10.1016/J.SEPPUR.2017.07.045.

[20] W.N.W. Salleh, A.F. Ismail, Carbon membranes for gas separation processes: recent progress and future perspective, J. Membr. Sci. Res. 1 (2015) 2–15, https://doi.org/10.22079/jmsr.2015.12301.

[21] N.W. Ockwig, T.M. Nenoff, Membranes for hydrogen separation, Chem. Rev. 107 (2007) 4078–4110, https://doi.org/10.1021/cr0501792.

[22] L. Hu, S. Pal, H. Nguyen, V. Bui, H. Lin, Molecularly engineering polymeric membranes for H2/CO2 separation at 100–300 °C, J. Polym. Sci. 58 (2020) 2467–2481, https://doi.org/10.1002/pol.20200220.

[23] M.J.T. Raaijmakers, M. Wessling, A. Nijmeijer, N.E. Benes, Hybrid polyhedral oligomeric silsesquioxanes–imides with tailored intercage spacing for sieving of hot gases, Chem. Mater. 26 (2014) 3660–3664, https://doi.org/10.1021/cm500691e.

[24] M.J.T. Raaijmakers, M.A. Hempenius, P.M. Schön, G.J. Vancso, A. Nijmeijer, M. Wessling, N.E. Benes, Sieving of hot gases by hyper-cross-linked nanoscale-hybrid membranes, J. Am. Chem. Soc. 136 (2014) 330–335, https://doi.org/10.1021/ja410047u.

[25] M.J.T. Raaijmakers, E.J. Kappert, A. Nijmeijer, N.E. Benes, Thermal imidization kinetics of ultrathin films of hybrid poly(POSS-imide)s, Macromolecules 48 (2015) 3031–3039, https://doi.org/10.1021/acs.macromol.5b00473.

[26] S. Neyertz, D. Brown, M.J.T. Raaijmakers, N.E. Benes, The influence of the dianhydride precursor in hyper-cross-linked hybrid polyPOSS-imide networks, Phys. Chem. Chem. Phys. 18 (2016) 28688–28703, https://doi.org/10.1039/C6CP06184B.

[27] L. Ansaloni, L. Deng, Advances in polymer-inorganic hybrids as membrane materials. Recent Dev. Polym. Macro, Micro Nano Blends Prep. Characterisation, 2016, pp. 163–206, https://doi.org/10.1016/B978-0-08-100408-1.00007-8.

[28] C.M. Zimmerman, W.J. Koros, Polypyrrolones for membrane gas separations. II. Activation energies and heats of sorption, J. Polym. Sci., Part B: Polym. Phys. 37 (1999) 1251–1265, https://doi.org/10.1002/(SICI)1099-0488(19990615)37:12<1251::AID-POLB6>3.0. CO;2-E.

[29] U. Beuscher, C.H. Gooding, The influence of the porous support layer of composite membranes on the separation of binary gas mixtures, J. Membr. Sci. 152 (1999) 99–116, https://doi.org/10.1016/S0376-7388(98)00205-1.

[30] A. Caravella, G. Barbieri, E. Drioli, Concentration polarization analysis in self-supported Pd-based membranes, Separ. Purif. Technol. 66 (2009) 613–624, https://doi.org/10.1016/J.SEPPUR.2009.01.008.

[31] T.A. Peters, M. Stange, H. Klette, R. Bredesen, High pressure performance of thin Pd–23%Ag/stainless steel composite membranes in water gas shift gas mixtures; influence of dilution, mass transfer and surface effects on the hydrogen flux, J. Membr. Sci. 316 (2008) 119–127, https://doi.org/10.1016/J.MEMSCI.2007.08.056.

[32] M.J.T. Raaijmakers, W. Ogieglo, M. Wiese, M. Wessling, A. Nijmeijer, N.E. Benes, Sorption behavior of compressed CO2 and CH4 on ultrathin hybrid poly(POSS-imide) layers, ACS Appl. Mater. Interfaces 7 (2015) 26977–26988, https://doi.org/10.1021/acsami.5b08286.